

Response of a rocksalt crystal to electromagnetic wave modeled by a multiscale field theory

Yajie Lei, James D. Lee* and Xiaowei Zeng

*Department of Mechanical and Aerospace Engineering,
The George Washington University, Washington, DC 20052, USA*

(Received August 19, 2008, Accepted December 1, 2008)

Abstract. In this work, a nano-size rocksalt crystal (magnesium oxide) is considered as a continuous collection of unit cells, while each unit cell consists of discrete atoms; and modeled by a multiscale concurrent atomic/continuum field theory. The response of the crystal to an electromagnetic (EM) wave is studied. Finite element analysis is performed by solving the governing equations of the multiscale theory. Due to the applied EM field, the inhomogeneous motions of discrete atoms in the polarizable crystal give rise to the change of microstructure and the polarization wave. The relation between the natural frequency of this system and the driving frequency of the applied EM field is found and discussed.

Keywords: atomic/continuum modeling; finite element; polarization; microstructure.

1. Introduction

In the framework of classical, non-relativistic theory, a description of the electromagnetic behavior of composite particles is introduced by Groot and Suttrop (1972). The field equations for the composite particles are expanded from the microscopic equations of the Maxwell-Lorentz field equations and the Newton equation with the Lorentz force inserted. Thereafter, from the viewpoint of classical continuum mechanics, a systematic and rational formulation of the electromagnetic theory of deformable and fluent bodies is presented by Eringen and Maugin (1980, 1990). Recently, Chung (2007), in a treatise of general continuum mechanics, introduces the electrodynamics, magnetohydrodynamics and electromagnetic waves for plasma.

Extended from classical continuum mechanics, the microcontinuum field theories, developed by Eringen (1999) and Eringen and Suhubi (1964), for material bodies possessing inner structures that can deform and interact with mechanical and electromagnetic field, cover a much broader range of important physical phenomena beyond those of classical field theories. The internal modes describing the stretching and distortion of the molecules extend the application of the continuum model to microscopic space/time scale. In this framework, Eringen (2003) further derived the linear constitutive relations for micromorphic electromagnetic-thermoelastic solids. It has been applied to study EM wave propagation in ferroelectric perovskites by Lee and Chen (2004).

For crystals having multiple atoms in a unit cell, physical response of the molecular crystal may

* Corresponding Author, jdlee@gwu.edu

be represented by homogeneous lattice deformation and by inhomogeneous internal atomic deformation. By decomposing these two deformations for microstructures, and by also decomposing momentum flux and heat flux into homogeneous and inhomogeneous parts, field representations of conservation laws at the atomic scale have been formulated in a newly developed multiscale field theory by Chen and Lee (2005, 2006), Chen *et al.* (2006) and Chen (2006). As a result of this formulation, a field representation of atomic many-body dynamics is obtained. The material is thus described as the combination of continuous collection of lattice points and a group of bonded atoms embedded within each lattice point. Based on this theory, the material system can thus be modeled as a continuum analyzed by finite element method with each point in the continuum representing a unit cell, which is made of a finite number of discrete atoms. Also, the constitutive relations are represented by the nonlinear and nonlocal interatomic forces. Moreover, the atomistic responses, such as optic phonon modes and polarization, can be described by the finite element analysis. Therefore, we call this model as a concurrent atomic/continuum model.

The multiscale field theory allows each atom to move arbitrarily within a unit cell and thus brings about the internal deformations. Therefore, it gives rise to the optical mode in phonon branches. Optical mode, as one type of wave propagation induced by the elastic distortions, essentially generates an electromagnetic field for a polarizable crystal. Moreover, polarization at the atomic-level only makes sense when defined in terms of the displacements of ions summed over a neutral stoichiometric unit, the smallest primitive unit cell in a crystal (Kittel 1967).

Within the multiscale field theory, the response in a microscopic continuum of rocksalt crystal *MgO* to an electromagnetic wave is simulated at atomic level. The finite element analysis based on the multiscale field theory is performed for this concurrent atomic/continuum system. The atomic unit is employed in this paper.

2. Governing equations and finite element formulation

The balance law for linear momentum in the multiscale field theory can be generally expressed as (Lee *et al.* 2007, Chen and Lee 2008)

$$\rho^\alpha \ddot{\mathbf{u}}^\alpha = \nabla_{\mathbf{x}} \cdot \mathbf{t}_{kin}^\alpha + \nabla_{\mathbf{y}^\alpha} \cdot \boldsymbol{\tau}_{kin}^\alpha + \mathbf{f}^\alpha / V^* + \boldsymbol{\varphi}^\alpha / V^* \quad (1)$$

where \mathbf{u}^α is the displacement of the α -th atom in a unit cell with its center located at \mathbf{x} ; \mathbf{y}^α is the position vector of the α -th atom relative to the center of the unit cell; ρ^α is the mass density of the α -th atom of a unit cell and V^* is the volume of that unit cell; \mathbf{t}_{kin}^α and $\boldsymbol{\tau}_{kin}^\alpha$ are the homogeneous and inhomogeneous kinetic parts of stresses which are proportional to temperature, respectively; \mathbf{f}^α and $\boldsymbol{\varphi}^\alpha$ are the forces acting on the α -th atom in that unit cell due to interatomic interactions and external fields, respectively. In the case of zero temperature, Eq. (1) is reduced to

$$m^\alpha \ddot{\mathbf{u}}^\alpha = \mathbf{f}^\alpha + \boldsymbol{\varphi}^\alpha \quad (2)$$

where $m^\alpha = \rho^\alpha V^*$ is the mass of atom α . The second term on the right hand side is the Lorentz force given by Jackson (1962),

$$\boldsymbol{\varphi}^\alpha = q^\alpha (\mathbf{E} + \mathbf{v} \times \mathbf{B} / c) \quad (3)$$

and q^α is the charge on atom α , c is the speed of light, \mathbf{E} is the electric field, \mathbf{B} is the magnetic field and \mathbf{v} is the velocity. Notice here, the rigid-ion model is adopted. The force due to interatomic

Table 1 Short-range interaction parameters for different pairs in MgO

Species α	Species β	$A^{\alpha\beta}$ (eV)	$\rho^{\alpha\beta}$ (\AA)	$C^{\alpha\beta}$ ($eV \cdot \text{\AA}^6$)
Mg^{2+}	Mg^{2+}	0.00	---	0.00
Mg^{2+}	O^{2-}	1284.380	0.2997	0.00
O^{2-}	O^{2-}	9547.960	0.2192	32.00

interactions is given by

$$\mathbf{f}^\alpha = -\sum_{\beta} \frac{\partial U_{\alpha\beta}(r_{\alpha\beta})}{\partial r_{\alpha\beta}} \cdot \frac{\mathbf{r}_{\alpha\beta}}{r_{\alpha\beta}} \quad (4)$$

Here the summation is over all β atoms, which have interactions with α atom and the empirical interatomic pair potential $U_{\alpha\beta}(r_{\alpha\beta})$ is the combination of long-range Coulomb interaction and short-range Buckingham potential,

$$U_{\alpha\beta}(r_{\alpha\beta}) = \frac{q^\alpha q^\beta}{r_{\alpha\beta}} + A_{\alpha\beta} e^{-r_{\alpha\beta}/\rho_{\alpha\beta}} - \frac{C_{\alpha\beta}}{r_{\alpha\beta}^6} \quad (5)$$

where $r_{\alpha\beta} = |\mathbf{r}_\alpha - \mathbf{r}_\beta|$ is the separation distance between atom α and atom β ; the parameters involved in the potential function, $A^{\alpha\beta}$, $\rho^{\alpha\beta}$ and $C^{\alpha\beta}$ are obtained through fitting to experimental results (Grimes 1994) and summarized in Table 1. This potential describes the energy composed by the long-range Coulomb energy, the repulsive energy by the Born-Mayer potential and the van der Waals attractive energy. The metal-metal interactions for metallic bonding, i.e., $Mg - Mg$ pair, is solely described by Coulomb potential. For other pairs, besides the long-range electrostatic Coulomb potential, the Born-Mayer potential describes the short-range metal-non-metal and non-metal – non-metal interactions for ionic bonding and covalent bonding respectively, i.e., $Mg - O$ and $O - O$ pairs. The van der Waals potential represents the correlated motions of electrons on different ions as a dipole-induced dipole interaction. It describes the dispersion interaction which becomes stronger as the atom or molecule becomes larger due to the increased polarizability of molecules with larger, more dispersed electron clouds. Therefore, it is only considered for $O - O$ pair. In this simulation, the long-range Coulomb forces are calculated through direct summation within this finite-size specimen. The cutoff used for the short-range interactions is 12\AA .

For the system with pair potential, by counting the interatomic forces acting on one atom coming from all other atoms, Eq. (2) can be rewritten as

$$m^\alpha \ddot{\mathbf{u}}(k, \alpha) = \sum_{l=1}^n \sum_{\beta=1}^v \mathbf{f}(k, \alpha; l, \beta) + \boldsymbol{\varphi}(k, \alpha) \quad (k = 1, 2, 3, \dots, n; \quad \alpha = 1, 2, 3, \dots, v) \quad (6)$$

where $\mathbf{f}(k, \alpha; l, \beta)$ is the interatomic force acting on the α -th atom of the k -th unit cell due to the interaction with the β -th atom of the l -th unit cell. The following is the finite-element formulation based on the governing equation Eq. (6).

The inner product of Eq. (6) with virtual displacement $\delta \mathbf{u}(k, \alpha)$ and the summation of the inner products over all α and k lead to

$$\begin{aligned} \sum_{k=1}^n \sum_{\alpha=1}^v m^\alpha \ddot{\mathbf{u}}(k, \alpha) \cdot \delta \mathbf{u}(k, \alpha) &= \sum_{k=1}^n \sum_{l=1}^n \sum_{\alpha=1}^v \sum_{\beta=1}^v \mathbf{f}(k, \alpha; l, \beta) \cdot \delta \mathbf{u}(k, \alpha) \\ &+ \sum_{k=1}^n \sum_{\alpha=1}^v \boldsymbol{\varphi}(k, \alpha) \cdot \delta \mathbf{u}(k, \alpha) \end{aligned} \quad (7)$$

Supposing we have N_e finite elements and each with 8 Gauss points, we can approximate Eq. (7) as

$$\begin{aligned} \sum_{I_e=1}^{N_e} \sum_{g=1}^8 \sum_{\alpha=1}^v \frac{J(I_e, g)}{V^*} \{ m^\alpha \ddot{\mathbf{u}}(I_e, g, \alpha) \cdot \delta \mathbf{u}(I_e, g, \alpha) - \boldsymbol{\varphi}(I_e, g, \alpha) \cdot \delta \mathbf{u}(I_e, g, \alpha) \\ - \frac{1}{2} \sum_{l=1}^n \sum_{\beta=1}^v \mathbf{f}(I_e, g, \alpha; l, \beta) \cdot [\delta \mathbf{u}(I_e, g, \alpha) - \delta \mathbf{u}(l, \beta)] \} = 0 \end{aligned} \quad (8)$$

where $J(I_e, g)$ is the Jacobian of the g -th Gauss point of the I_e -th element; $\mathbf{f}(I_e, g, \alpha; l, \beta)$ is the force acting on the α -th atom in the unit cell located at the g -th Gauss point of the I_e -th element due to the interaction with the β -th atom of the l -th unit cell. Here, instead of the integral, the summation is employed in this generalized finite element formulation. It is our idea to use the Jacobian divided by the volume of the unit cell $J(I_e, g)/V^*$, which is a dimensionless quantity, to represent the number of unit cells associated with the g -th Gauss point of the I_e -th element. Notice that $J(I_e, g)/V^*$ is a constant in time even in the case of large deformation. Actually, $J(I_e, g)/V^*$ being constant in time is the law of conservation of mass at the atomic level. Meanwhile, in the derivation of Eq. (8), we have utilized

$$\sum_{k=1}^n \sum_{l=1}^n \sum_{\alpha=1}^v \sum_{\beta=1}^v \mathbf{f}(k, \alpha; l, \beta) \cdot \mathbf{u}(k, \alpha) = \sum_{k=1}^n \sum_{l=1}^n \sum_{\alpha=1}^v \sum_{\beta=1}^v \mathbf{f}(l, \beta; k, \alpha) \cdot \mathbf{u}(l, \beta) \quad (9)$$

and

$$\mathbf{f}(k, \alpha; l, \beta) = -\mathbf{f}(l, \beta; k, \alpha) \quad (10)$$

Finally, through the shape functions

$$\delta \mathbf{u}(I_e, g, \alpha) = \sum_{\lambda=1}^8 N^\lambda(g) \delta \mathbf{U}^\alpha(I_e, \lambda), \quad \delta \mathbf{u}(l, \beta) = \sum_{\lambda=1}^8 N^\lambda(l) \delta \mathbf{U}^\beta(l, \lambda) \quad (11)$$

and the connectivity of the finite element model

$$I_p(\lambda) \equiv IJK(\lambda, I_e), \quad J_p(\lambda) \equiv IJK(\lambda, l) \quad (12)$$

where $N^\lambda(g)$ and $N^\lambda(l)$ are the values of the λ -th shape function evaluated at the g -th Gauss point of the I_e -th element and the center of the l -th unit cell, respectively; $\delta \mathbf{U}^\alpha(I_e, \lambda)$ and $\delta \mathbf{U}^\beta(l, \lambda)$ are the virtual displacements of the α -th and the β -th atoms of the λ -th node of the I_e -th element and the element where the l -th unit cell is located, respectively; $IJK(\lambda, I_e)$ and $IJK(\lambda, l)$ are the global nodal numbers of the λ -th node of the I_e -th element and the element that the l -th unit cell is located, respectively. Now, Eq. (8) can be written as

$$\sum_{I_e=1}^{N_e} \sum_{g=1}^8 \sum_{\alpha=1}^{\nu} \sum_{\lambda=1}^8 \frac{J(I_e, g)}{V^*} \{N^\lambda(g)[m^\alpha \ddot{\mathbf{u}}(I_e, g, \alpha) - \boldsymbol{\varphi}(I_e, g, \alpha)] \cdot \delta \mathbf{U}^{I_p(\lambda), \alpha} - \frac{1}{2} \sum_{l=1}^n \sum_{\beta=1}^{\nu} \mathbf{f}(I_e, g, \alpha; l, \beta) \cdot [N^\lambda(g) \delta \mathbf{U}^{I_p(\lambda), \alpha} - N^\lambda(l) \delta \mathbf{U}^{J_p(\lambda), \beta}]\} = 0 \quad (13)$$

Going through the process of assembly properly, one may rewrite Eq. (13) as

$$\sum_{I_e=1}^{N_e} \sum_{g=1}^8 \sum_{\alpha=1}^{\nu} \sum_{\lambda=1}^8 \sum_{\mu=1}^8 \frac{J(I_e, g)}{V^*} N^\lambda(g) N^\mu(g) m^\alpha \ddot{\mathbf{U}}^{I_p(\mu), \alpha} \cdot \delta \mathbf{U}^{I_p(\lambda), \alpha} = \sum_{I_p=1}^{N_p} \sum_{\alpha=1}^{\nu} \{\mathbf{F}^{I_p, \alpha} + \boldsymbol{\varphi}^{I_p, \alpha}\} \cdot \delta \mathbf{U}^{I_p, \alpha} \quad (14)$$

where $\mathbf{F}^{I_p, \alpha}$ and $\boldsymbol{\varphi}^{I_p, \alpha}$ are the forces due to interatomic interactions and external fields, respectively, acting on the α -th atom of the I_p -th node; $\delta \mathbf{U}^{I_p, \alpha}$ is the virtual displacement of the α -th atom of the I_p -th node. Eq. (14) is thereby the set of second order ordinary differential equations, which is solved by central difference method in the numerical implementation of this work. Further, the inhomogeneous motion of arbitrary atoms in the system can be described through the nodal values and shape functions.

3. Finite element model and simulation results

In the current atomic/continuum model, each finite element contains a large number of lattice points, and according to the specific meshes, the number of lattice points within each element may vary. The lattice point is defined as the mass center of the unit cell. In this model for each element, the Gauss point is located right at a lattice point and other lattice points within this element are distributed evenly as in a single crystal around the Gauss point. Thus, the atoms associated with the lattice points are filling the whole specimen. Based on this model, a 3D finite nano-size *MgO* specimen shown in Fig. 1(a) is investigated in this work. Because the EM wave is considered to propagate along the x-direction, 9 cubic elements are linearly arranged along the x-axis by design. The size of each element is $80 \times 80 \times 80 \text{ Bohr}^3$ ($7.6 \times 10^4 \text{ \AA}^3$). The rocksalt lattice structure, shown in Fig. 1(b), with lattice constant $a = b = c = 7.94 \text{ Bohr}$, crystallized as the initial configuration and filled the finite element model. There are 4 *Mg* cations represented by open circles and 4 *O* anions represented by solid circles per unit cell. In this specimen there are 9 finite elements and 8 Gauss points in each element; the dimensionless quantity $J(I_e, g)/V^*$ represents 9217 unit cells, i.e., $9217 \times 8 = 73736$ atoms.

We consider a given electromagnetic wave propagating in the specimen. The initial displacement and velocity of each node are zero; no loading and no boundary constraints are applied in the simulation. The induced body force, i.e., the Lorentz force acting on the charged atoms, is caused solely by the external EM field. The polarization response can be schematically illustrated by Fig. 2. Driven by the Lorentz force, according to Eq. (3), the charged ions Mg^{2+} and O^{2-} in this specimen will move along z-direction first with the velocity v_z induced by the applied electric field E_z . This

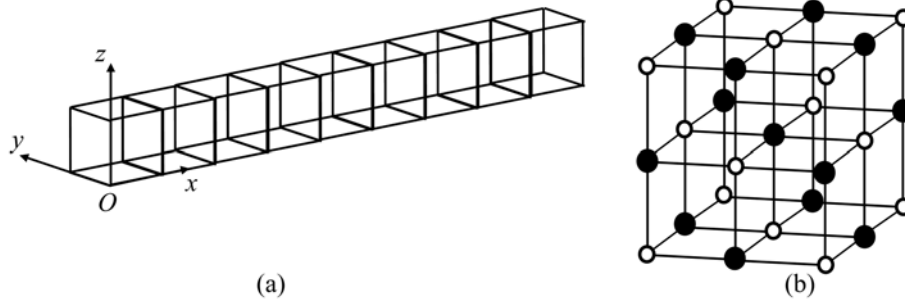


Fig. 1 (a) The finite element model of the specimen ($9 \times 1 \times 1$ elements); each element is a $80 \times 80 \times 80$ a. u.³ = 7.6×10^4 Å³ cube; the total number of atoms is 73736 (9217 unit cells) and the initial configuration is constructed with rocksalt structure; (b) The rocksalt structure of *MgO*; the solid circles represent *Mg* cations and the open circles represent *O* anions; each unit cell has 8 atoms

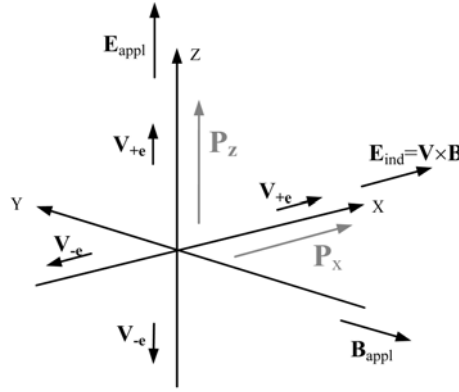


Fig. 2 The schema to illustrate the polarization response in the specimen to the applied EM field

motion gives rise to polarization P_z . Then, due to the motion of ions in z -direction and the applied magnetic field along the negative y -direction, B_y , a Lorentz force, equal to $q^{\alpha} \mathbf{v} \times \mathbf{B} / c$ arises in x -direction. Hence, the charged ions will move in x -direction that generates polarization P_x as well.

The harmonic electric field $\mathbf{E} = [E_x \ E_y \ E_z] = [0 \ 0 \ E_z]$ and magnetic field $\mathbf{B} = [B_x \ B_y \ B_z] = [0 \ B_y \ 0]$ with variance in time and space are applied with

$$E_z = -B_y = \begin{cases} A \exp[i\omega(x - ct)/c], & \text{if } t \leq t_w \\ 0, & \text{if } t > t_w \end{cases} \quad (15)$$

where speed of light $c = 137.036 \hbar a_0^{-1} m_e^{-1}$, $A = 0.01 \hbar^2 e^{-1} a_0^{-3} m_e^{-1}$. Total simulation time of this work $t_f = 30000 a_0^2 m_e \hbar^{-1}$ and applied EM field lasts up to $t_w = 10000 a_0^2 m_e \hbar^{-1}$. The driving frequency ω applied to the system is considered for two different cases: case I (high frequency) $\omega = \omega_1 = 4 \times 10^{-3} \pi \text{ rad} \cdot (a_0^2 m_e \hbar^{-1})^{-1}$ and case II (low frequency) $\omega = \omega_2 = 4 \times 10^{-4} \pi \text{ rad} \cdot (a_0^2 m_e \hbar^{-1})^{-1}$.

At atomic-level computations, classically, the polarization \mathbf{P} is defined as the dipole moment per unit volume (Kittel 1967),

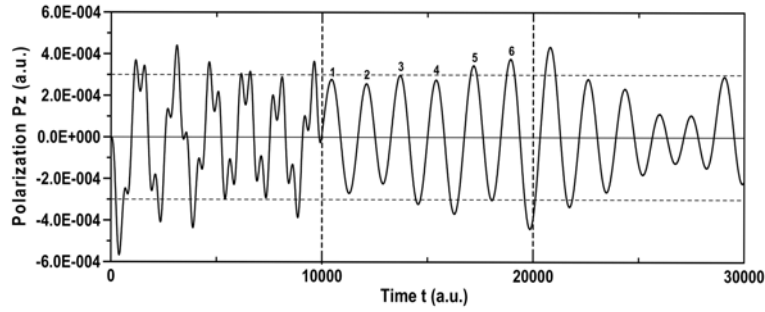
$$\mathbf{P} = \frac{e}{V^*} \sum_n Z_n \mathbf{R}_n \quad (16)$$

where \mathbf{R}_n is the position vector of charge Z_n , e is the unit of charge, V^* is the volume of unit cell.

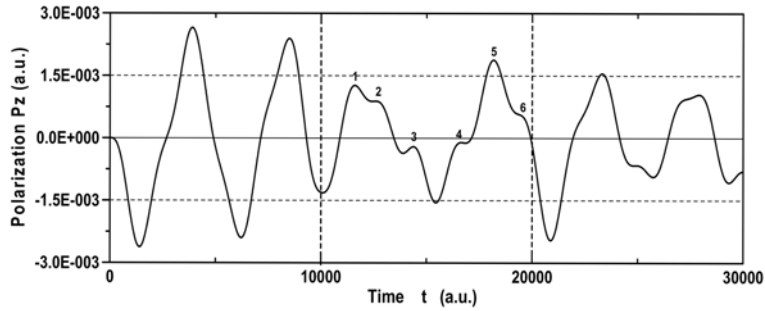
Using a rigid-ion model to describe a lattice system, we assume that the ionic charges are approximated by the point charges centered at the nuclei, in other words, the ions are not polarizable. Consequently, the polarization of the lattice system has the form given by the field representation in the multiscale field theory (Chen *et al.* 2006)

$$\mathbf{P} = \mathbf{P}(\mathbf{x}, t) = \sum_{k=1}^n \sum_{\alpha=1}^{\nu} q^{\alpha} \mathbf{u}^{k\alpha}(t) \delta(\mathbf{R}^k - \mathbf{x}) \quad (17)$$

Here, q^{α} is the charge of the α -th atom; $\mathbf{u}^{k\alpha}$ is the displacement of the α -th atom in the k -th unit cell with respect to the reference state, $\mathbf{u}^{k\alpha} = \mathbf{R}^{k\alpha} - \mathbf{R}_o^{k\alpha}$; the delta function in Eq. (17) is a localization function that provides the link between the phase space and the physical space descriptions. By summing k and α over the number of unit cells n and the number of atoms ν within each unit cell, Eq. (17) can give us both the local property and bulk one for a finite size specimen. With Eq. (14), from the compute program, we get the displacements of each atom of all the finite element nodes. Based on that, we calculate the polarization.



(a)

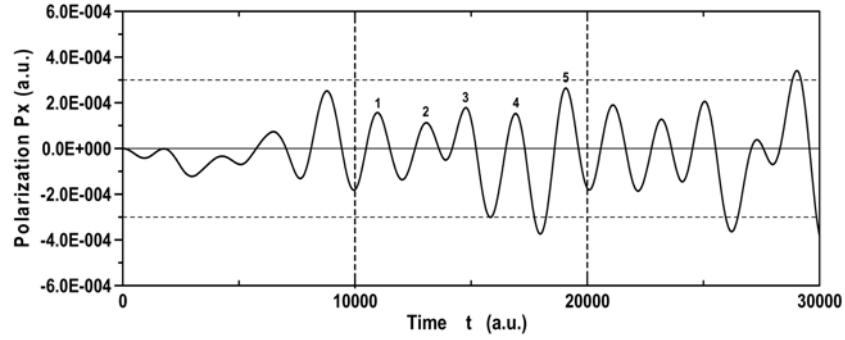


(b)

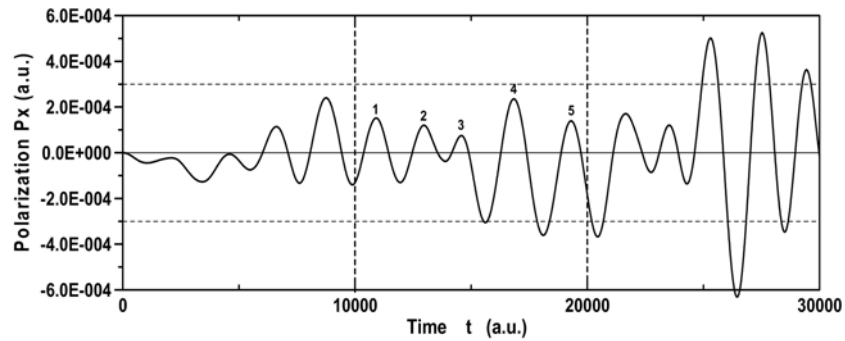
Fig. 3 The polarization P_z ($\hbar^2 e^{-1} m_e^{-1}$) of the $y-z$ plane at $x=0$ as a function of time $t(a_0^2 m_e \hbar^{-1})$. Driving frequency (a) $\omega_1 = 4 \times 10^{-3} \pi \text{ rad} \cdot (a_0^2 m_e \hbar^{-1})^{-1}$; (b) $\omega_2 = 4 \times 10^{-4} \pi \text{ rad} \cdot (a_0^2 m_e \hbar^{-1})^{-1}$

According to Eq. (17), the polarization density $\mathbf{P}(\mathbf{x}, t)$ can be calculated as a vector-valued function of space and time. The polarizations P_z and P_x of the $y-z$ cross section at $x = 0$ are plotted as function of time for high-frequency case $\omega_1 = 4 \times 10^{-3} \pi \text{ rad} \cdot (a_0^2 m_e \hbar^{-1})^{-1}$ and low-frequency case $\omega_2 = 4 \times 10^{-4} \pi \text{ rad} \cdot (a_0^2 m_e \hbar^{-1})^{-1}$ in Fig. 3 and Fig. 4, respectively. Notice that in the simulation there are two stages divided at $t = t_w = 10000 a_0^2 m_e \hbar^{-1}$; in the second stage $t \geq t_w$, the external EM wave propagation is terminated.

When time $t \leq t_w$, along z -direction, Fig. 3 presents the distinct response of polarization P_z to the applied EM wave with different driving frequency. We found that two patterns of coupling between the driving frequency and the natural frequency of the system. In Fig. 3 (a), the applied high-frequency electric field E_z drives P_z to show a larger frequency compared to its natural frequency, while it constrains the magnitude of P_z . In contrast, in Fig. 3 (b), the applied low-frequency E_z obviously reduces the frequency of P_z and naturally makes P_z reach a significant larger magnitude. These two responses indicate that the internal deformation of microstructure is crucially influenced by the driving frequency of the applied external EM field. Relative to the natural frequency of this polarizable system, the lower driving frequency can make larger internal deformation, namely higher polarization.



(a)



(b)

Fig. 4 The polarization $P_x (\hbar^2 e^{-1} m_e^{-1})$ of the $y-z$ plane at $x = 0$ as a function of time $t (a_0^2 m_e \hbar^{-1})$. Driving frequency (a) $\omega_1 = 4 \times 10^{-3} \pi \text{ rad} \cdot (a_0^2 m_e \hbar^{-1})^{-1}$; (b) $\omega_2 = 4 \times 10^{-4} \pi \text{ rad} \cdot (a_0^2 m_e \hbar^{-1})^{-1}$

When time $t > t_w$, there is no external field, damping force or boundary constraint acting on this system, only the interatomic body force exists. Then the effect of the EM wave disappears and the response of polarization keeps its natural frequency of the specimen irrespective of what has been applied when $t \leq t_w$. Both Figs. 3 (a) and (b) show that P_z has six peaks generated during every time interval of 1.0×10^4 atomic units.

Unlike P_z , when time $t \leq t_w$, the polarization in x-direction P_x induced by the Lorentz force $q^\alpha v_z B_y / c$ shows the similar response to the external fields with different driving frequencies, see Figs. 4 (a) and (b). Moreover, the polarization P_x consistently has a vibration frequency close to its natural frequency in both cases. When $t > t_w$, considered as another natural frequency in x-direction distinct from P_z , five peaks are found at the same time interval for P_x . The difference in the magnitude of P_x between the two cases is much small relative to that of P_z . It is considered as the effect from noise and accumulated error.

In contrast with the classical molecular dynamics simulations, the method employed in this work reveals its particular advantages. First, the finite nano-size specimen is modeled without any periodic boundary conditions. This makes an exact physical model for simulating wave propagations. Second, by solving the field equation, the local and instantaneous property obtained in this simulation has physical meaning without the need of taking any statistical average. Third, using finite element analysis within the multiscale field theory, the simulation is computationally more efficient. This field theory allows the size of each finite element to be arbitrarily built from nanoscopic to microscopic. The enlarged elements involving more atoms enable the problem to be scaled up. Of course, it will cause the compromise of accuracy. To get accurate solution, more small-sized elements are needed, which implies more computing effort and cost are needed. Therefore, for specific problems, computer software of this work enables us to make a flexible choice between the system size and computing efficiency.

4. Summary

Through a multiscale field theory, the internal deformation of the microstructure in a nano-size continuum under the influence of an applied external EM field is investigated. The atomic-level behavior of this polarizable system is demonstrated by finite element analyses performed on the concurrent atomic/continuum model. The simulation results are summarized as follows:

(1) The polarization response indicates that there is an obvious coupling between the driving frequency of the applied EM field and the natural frequency of the system, but only in the direction of the electric field applied.

(2) The frequency of the external field is a crucial factor. The external field with lower driving frequency relative to the natural frequency of the polarizable system causes larger internal deformation, hence higher polarization.

(3) After the EM wave propagation was terminated, the polarization response goes on with its natural frequency irrespective of what has been applied before.

Acknowledgments

This work is supported by the National Science Foundation under Grant Number CMMI-0646674.

References

- Chen, Y. (2006), "Local stress and heat flux in atomistic systems involving three-body forces", *J. Chem. Phys.*, **124**, 054113-1-054113-6.
- Chen, Y. and Lee, J. D. (2005), "Atomistic formulation of a multiscale theory for nano/micro physics", *Philosophical Mag.*, **85**, 4095-4126.
- Chen, Y. and Lee, J. D. (2006), "Conservation laws at nano/micro scales", *J. Mech. Mater. Struct.*, **1**, 681-704.
- Chen, Y. and Lee, J. D. (2008), "Multiscale computation for nano/micro materials", *ASCE J. Eng. Mech.*, submitted for publication.
- Chen, Y., Lee, J. D., Lei, Y. and Xiong, L. (2006), "A multiscale field theory: Nano/micro materials", *Multiscale in Molecular and Continuum Mechanics* (edited by G. C. Sih), Springer, New York, 23-65.
- Chung, T. J. (2007), *General Continuum Mechanics*, Cambridge University Press, New York.
- Eringen, A. C. (1980), *Mechanics of Continua*, R. E. Krieger Publishing Co., Malabar, Florida.
- Eringen, A. C. (1999), *Microcontinuum Field Theories I: Foundations and Solids*, Springer-Verlag, New York.
- Eringen, A. C. (2003), "Continuum theory of micromorphic electromagnetic thermoelastic solids", *Int. J. Eng. Sci.*, **41**, 653-665.
- Eringen, A. C. and Maugin, G. A. (1990), *Electrodynamics of Continua I: Foundations and Solid Media*, Springer-Verlag, New York.
- Eringen, A. C. and Suhubi, E. S. (1964), "Nonlinear theory of simple micro-elastic solids-I", *Int. J. Eng. Sci.*, **2**, 189-203.
- Grimes, R. W. (1994), "Solution of MgO, CaO, and TiO₂ in α -Al₂O₃", *J. Am. Ceram. Soc.*, **77**, 378-384.
- Groot, S. R. de and Suttrop, L. G. (1972), *Foundations of Electrodynamics*, North-Holland, Amsterdam.
- Jackson, J. D. (1962), *Classical Electrodynamics*, Wiley, New York.
- Kittel, C. (1967), *Introduction to Solid State Physics*, John Wiley & Sons Inc., New York.
- Lee, J. D. and Chen, Y. (2004), "Electromagnetic wave propagation in micromorphic elastic solids", *Int. J. Eng. Sci.*, **42**, 841-848.
- Lee, J. D., Chen, Y., Xiong, L., Lei, Y., Zeng, X. and Deng, Q. (2007), "Theoretical development, finite element formulation and application of a multiscale continuum field theory", *Proceeding of the 18th Engineering Mechanics Division Conference of ASCE*, Blacksburg, June.